Derived Optimal Linear Combination Evapotranspiration (DOLCE): a global gridded synthesis ET estimate

Sanaa Hobeichi[1,2], Gabriel Abramowitz[1,2], Jason Evans[1] and Anna Ukkola[2]

[1] Climate Change Research Centre, University of New South Wales, Sydney, NSW 2052, Australia
[2] ARC Centre of Excellence for Climate System Science, University of New South Wales, Sydney, NSW 2052, Australia

Correspondence to: Sanaa Hobeichi (s.hobeichi@student.unsw.edu.au)

Abstract. Accurate global gridded estimates of evapotranspiration (ET) are key to understanding water and energy budgets, as well as being required for model evaluation. Several gridded ET products have already been developed which differ in their data requirements, the approaches used to derive them and their estimates, yet it is not clear which provides the most reliable estimates. This paper presents a new global ET dataset and associated uncertainty with monthly temporal resolution for 2000–2009. Six existing gridded ET products are combined using a weighting approach trained by observational datasets from 159 FLUXNET sites. The weighting method is based on a technique that provides an analytically optimal linear combination of ET products compared to site data, and accounts for both the performance differences and error covariance between the participating ET products. We examine the performance of the weighting approach in several in-sample and out-of-sample tests that confirm that point-based estimates of flux towers provide information at the grid scale of these products. We also provide evidence that the weighted product performs better than its six constituent ET product members in three common metrics. Uncertainty in the ET estimate is derived by rescaling the spread of participating ET products so that their spread reflects the ability of the weighted mean estimate to match flux tower data. While issues in observational data and any common biases in participating ET datasets are limitations to the success of this approach, future datasets can easily be incorporated and enhance the derived product.

1 Introduction

Improving the accuracy and understanding of uncertainties in the spatial and temporal variations of Evapotranspiration (ET) globally is key to a number of endeavours in climate, hydrological and ecological research. Its estimation is critical to water resource, heatwave and ecosystem stress prediction and it provides constraint on the energy, water and carbon cycles. For these reasons, it is also useful for evaluating the performance of land surface models (LSMs). To identify LSM performance issues and diagnose their probable causes, the observed values of LSM inputs and outputs need to be known with sufficient accuracy and precision. At the site scale, FLUXNET (Baldocchi et al., 2001; Baldocchi, 2008), a global group of tower sites that measures the exchange of energy, water and carbon between the land surface and the atmosphere, provides direct observations of ET and most of the drivers and outputs of LSMs with quantifiable uncertainty and sufficient accuracy to

make diagnostic evaluation possible. This fact has led to a range of model evaluation, comparison and benchmarking studies using FLUXNET data (e.g. Abramowitz, 2005, 2012; Best et al., 2015; Chen et al., 1997; Stöckli et al., 2008; Wang et al., 2007). Haughton et al. (2016) clearly showed that the flux tower data quality is good enough to provide diagnostic constraint on LSMs at the site scale. However, the point scale is not the spatial scale at which these models are typically used. In either

5 climate projections or weather forecast applications, gridded model estimates are required at the regional or global scale, with grid cell surface areas of order 25 km^2–40 000 km^2. The relevance of model diagnostic information at the site scale to broader scale gridded simulations remains unclear.

The advancement of remote sensing technology and satellite image processing techniques has dramatically improved the estimation of many components of LSM forcing (e.g. surface air temperature, precipitation, radiation components and

10 vegetation properties) (Loew et al., 2016). Together with the reasonable density of in-situ surface observations, this has meant that reanalysis products – usually the basis of gridded land surface forcing data sets at regional and global scales – are reasonably well constrained. On the other hand, very few LSM outputs (such as evapotranspiration or sensible heat flux) can be directly observed by remote sensing, and the only currently available way to derive them is by the use of modelling schemes or empirical formulations that use satellite based datasets (Jung et al., 2011; Fisher et al., 2008; Miralles et al.,

15 2011b; Martens et al., 2016; Mu et al., 2007; 2011; Su, 2002; Zhang et al., 2016; 2010). This approach leads to large and usually unquantifiable uncertainties. As a result, gridded LSM evaluation products show considerable differences (Ershadi et al., 2014; Jiménez et al., 2011; McCabe et al., 2016 ; Michel et al., 2016; Vinukollu et al., 2011). If an accurate description of these uncertainties was available, then it might be possible to evaluate gridded LSM simulations in certain circumstances, but until now very few studies quantify LSM uncertainties at regional or global scales (Badgley et al., 2015; Loew et al.,

20 2016; Zhang et al., 2016).

Several gridded ET products have already been developed (see Table 1). These ET products differ in their data requirements, the approaches used to derive them and their estimates (Wang and Dickinson, 2012). So far, it is not at all clear which product provides the most reliable estimates. Recently, inter-comparison studies have aimed to evaluate and compare the available gridded ET products. For instance, Vinukollu et al. (2011), ran simulations of the Surface Energy Balance System

25 SEBS, Penman–Monteith scheme by Mu (PM-Mu) and modified Priestley–Taylor (PT–JPL) forced by a compiled gridded dataset. The monthly model ET estimates were then compared with ET observations from 12 eddy-covariance towers. The root mean square deviation (RMSD) and biases for all the models fell within a small range with the highest correlation with tower data for PT–JPL, and the lowest for SEBS. These results somewhat disagree with the work of Ershadi et al. (2014) who inspected the performance of SEBS, the single-source Penman–Monteith, advection-aridity (AA) complementary

30 method (Brutsaert and Stricker, 1979) and PT–JPL using a high quality forcing dataset from 20 FLUXNET stations and found that the models can be ranked from the best to the worst model as: PT–JPL followed closely by SEBS then PM and finally AA. In the same study, a more detailed analysis revealed that no single model was consistently the best across all landscapes. More recently, in the Energy and Water cycle Experiment (GEWEX) LandFlux project, McCabe et al. (2016) ran simulations of the algorithms in SEBS, PT–JPL, PM-Mu and Global Land Evaporation Amsterdam Model (GLEAM)

from common global-scale gridded forcing data, as well as site-based forcing data, and assessed their response relative to ET measurements from forty-five globally distributed FLUXNET towers. The results indicated that PT–JPL achieved the highest statistical performance, followed closely by GLEAM, whereas PM-MU and SEBS tended to under- and over-estimate fluxes respectively. Furthermore, in the Water Cycle Multi-mission Observation Strategy for Evapotranspiration

5 (WACMOS-ET) project-part 1, Michel et al. (2016) carried out validation experiments for PT–JPL, PM-MU, SEBS and GLEAM against in situ measurements from 85 FLUXNET tower data and found that there was no single best performing model.

In each of the evaluation studies described above, gridded ET data sets are "ground-truthed" using flux tower data from FLUXNET by comparing grid cell values to those measured at the site scale. Most gridded ET products have a 0.5-degree

10 resolution, so that each grid cell can represent an area of around 2500 km^2. The fetch of flux tower measurements varies depending on terrain, vegetation and weather, but is typically under 1 km^2 (Burba and Anderson, 2010) . None of these studies directly address this obvious scale mismatch, and the degree to which surface heterogeneity might nullify any information that flux towers provide about fluxes at these larger scales. Indeed, all the evaluation studies that compared gridded estimates against flux tower observations highlighted this point as a limitation in the evaluation approach.

15 Zhang et al. (2016) pointed out that merging an ensemble of gridded ET products using a sophisticated data fusion method is likely to generate a better ET product with reduced uncertainty. Ershadi et al. (2014) and McCabe et al. (2016) noted in their studies that the multi-product mean produces improved estimates relative to individual ET products. Similarly, the analysis result of the LandFlux-EVAL project (Mueller et al., 2013) suggested that deriving ET values using the mean of multiple datasets outperforms the ET values from individual datasets. These results do suggest that flux towers likely provide some

20 information at the gridded scale, since there are solid theoretical reasons to expect the mean to outperform individual estimates (Annan and Hargreaves, 2010; Bishop and Abramowitz, 2013), although this fact was not noted in these studies. That is, we would expect that the mean of a range of relatively independent approaches – whose errors are somewhat uncorrelated – would provide a better estimate to observations if those observations were of the same system being simulated. In this study we provide an even stronger vindication of this relationship.

25 This paper introduces a new method for deriving globally gridded ET as well as its spatio-temporal uncertainty by combining existing gridded ET estimates. The method is based on the ensemble weighting and rescaling technique suggested by Bishop and Abramowitz (2013). The technique provides an analytically optimal linear combination of ensemble members that minimizes mean square error when compared to an observational dataset, and so accounts for both the performance differences and error covariance between the participating ET products (for example, caused by the fact that different ET

30 datasets might share a forcing product). In this way, at least in-sample, the optimal linear combination is insensitive to the addition of redundant information. We use a broad collection of FLUXNET sites as the observational constraint.

We examine the performance of the weighting approach in several in-sample and out-of-sample tests that confirm flux towers do indeed provide information at the grid scale of these products. Having confirmed this, we note that this "Derived

Optimal Linear Combination Evapotranspiration" (DOLCE) is more observationally constrained than the individual participating gridded ET estimates and therefore provides a valuable addition to currently available gridded ET estimates. Sect. 2.1 and 2.2 present the gridded ET data sets and the flux tower ET used to derive the weighted ET product. Sect. 2.3 describes the weighting approach used to calculate the linear combination ET and its uncertainty. In Sect. 2.4 we explain our

5   methods for testing the weighting approach and the representativeness of the point scale to the grid scale. We then present and discuss our results in Sect. 3 and 4 before concluding.

2 Methods, data and experimental setup

To build the DOLCE product, six global gridded ET products, all classified as diagnostic datasets based on Mueller et al. (2011), are weighted based on their ability to match site-level data from 159 globally distributed flux tower sites. DOLCE is

10   derived at 0.5° spatial resolution and monthly temporal resolution for 2000–2009.

2.1 ET datasets

This study employs monthly values from ten existing gridded ET datasets (Table 1). Only six of these datasets – referred to in this study as the Diagnostic Ensemble – are used for building DOLCE, while all of the ten are used to evaluate its performance (we'll refer to these as the Reference Ensemble). The reasons for restricting the Diagnostic Ensemble are (a) to

15   maximize the time period covered by DOLCE (see Table 1), (b) maximize the number of flux tower sites that can inform the weights (noting that datasets have different spatial coverage), and (c) to avoid LSM-based estimates in the final DOLCE product, so that its validity for LSM evaluation is clearer. For these reasons, CSIRO-global, LandFlux-EVAL-ALL, LandFlux-EVAL-DIAG and PT–JPL were removed from the Diagnostic Ensemble.

The weighting approach becomes increasingly effective as more products are included in the weighted mean, but since

20   different products have different spatial coverage, there is a need to strike a balance between maximizing the number of products included in DOLCE and maximizing spatial coverage of DOLCE. To resolve this issue, three different subsets of the Diagnostic Ensemble were chosen to derive DOLCE "tiers". The three DOLCE tiers differ in their spatial coverage of ET and uncertainty, the number of ET products included, and the number of flux towers employed to compute them. DOLCE tier 1 was derived by employing all the products in the Diagnostic Ensemble and 138 sites, and has a spatial coverage equal

25   to the intersection of the global land covered by these products, as shown in Red in Fig. 1. In DOLCE tier 2, GLEAM v2B was excluded and the remaining products were used to compute ET and uncertainty, increasing the spatial coverage and allowing 151 observational flux tower sites. The newly added regions in DOLCE tier 2 are shown in orange in Fig. 1. Finally, ET and uncertainties in the regions shown in yellow were computed using only two ET products, GLEAM V2A and GLEAM V3A, to create DOLCE tier 3, using 159 flux sites. With this approach, we manage to create a global product

30   without sacrificing data quality in regions where more information is available.

2.2 Flux tower data

The flux tower data used in this work is a composite of daily values from the FLUXNET2015-Tier 1 (FN) and LaThuile2007 (LT) Free Fair Use databases ((Baldocchi, 2008; Baldocchi et al., 2001; Papale et al., 2012; ORNL DAAC, 2015, www.fluxdata.org). We applied quality control and filtering to the site data as follows:

5   1.   Omit the observations that don't fall within the temporal coverage of DOLCE

2.   Omit the daily ET observations if less than 50% of half-hourly ET was observed (as opposed to gap-filled)

3.   Omit the monthly ET aggregates that have been calculated from less than 15 daily mean ET values.

4.   Correct the remaining site-months of ET observations from the LT dataset for energy balance non-closure on a site-by-site basis (energy closure corrected FN daily data was used)

10   5.   Keep only the sites that are located within the spatial coverage of products in the three tiers of the Diagnostic Ensemble (Fig. 2).

6.   Exclude irrigated sites or those that have only one monthly record.

Applying (1), (2) and (3) reduced the number of tower sites that were available at the beginning of the analysis from 246 to 172 sites, and produced a total of 7891 site-months (out of a possible 18468). Applying (5) and (6) reduced the number of

15   sites against which the weighting is tested to 138 sites in DOLCE tier 1, increasing to 151 sites in DOLCE tier 2 and 159 in DOLCE tier 3. In (4), two different correction techniques where applied for energy balance non-closure at LaThuile sites. Both involve ensuring that $R_n - G = H + LE$ where R_n is the net radiation, G, H and LE are the ground heat flux, sensible heat flux and latent heat flux respectively, at either the monthly timescale or over the length of the entire site record.

The first correction method distributes the residual errors in heat fluxes according to the Bowen (Bowen, 1926; Sumner and

20   Jacobs, 2005; Twine et al., 2000)   such that:

$$BR = \frac{H_{uncorrected}}{LE_{uncorrected}}$$

is applied using

$$F_{corrected} = \frac{R_n - G}{H_{uncorrected} + LE_{uncorrected}} \times F_{uncorrected}$$

where F is either H or LE, so that BR is unchanged between corrected and uncorrected fluxes. At first, the Bowen Ratio

25   technique was applied on monthly basis, but this occasionally seemed to give erratic results in the corrected flux values. However, when a single correction per site was applied across all the monthly records, the results were more consistent.

The second approach calculates ET as the Residual term in the Energy Balance Equation $LE_{corrected} = R_n - H - G$. The two correction methods were tested separately but no qualitative differences were noticed. All results below use the BR technique.

2.3 Weighting approach

The weighting approach presented here was suggested by Bishop and Abramowitz (2013). Given an ensemble of ET estimates and a corresponding observational dataset across time and space, the weighting builds a linear combination of the ensemble members that minimizes the mean square difference (MSD) with respect to the observational dataset such that: If

5 x_k^j is the jth time-space step of the kth bias-corrected ET product (i.e after subtracting the mean error from the product), and a linear combination of the ET estimates is expressed as

$$\mu_e^j = w^T x^j = \sum_{k=1}^{K} w_k x_k^j \quad , \tag{1}$$

then the weights w^T provide an analytical solution to the minimization of

$$\sum_{j=1}^{J} (\mu_e^j - y^j)^2$$

10 subject to the constraint that $\sum_{k=1}^{K} w_k = 1$, where $j \in [1, J]$ are the space and time steps, $k \in [1, K]$ represent the ET products, y^j is the jth observed space-time step.

The solution is expressed as $w = \frac{A^{-1} 1}{1^T A^{-1} 1}$, where $1^T = \overbrace{[1,1,\dots,1]}^{\text{k elements}}$ and A is the k×k error covariance matrix of the gridded products. Further details are in Bishop and Abramowitz (2013) and Abramowitz and Bishop (2015).

As noted above, this weighting approach has two key advantages. 1) It provides an optimal solution to minimizing mean

15 square error differences between the weighted ET estimates and the observational tower data in-sample. 2) It accounts for the error covariance between the participating datasets (e.g. caused by the fact that single datasets may share ET schemes or forcing), that is, they may not provide independent estimates. The analytical solution guarantees that the weighted mean will perform as well or better than the unweighted mean or any individual estimate included in the linear combination, at least on the data used to train the weights (that is, in-sample). Moreover, the addition of a new gridded ET product to the ensemble

20 will not degrade the performance of the weighted product, even if it consists of a duplicate product or a poor performing product. In order to confirm this in-sample weighting improvement, we performed an in-sample test presented in the supplementary material (Fig. S1). However, there is no guarantee that the weighted product will necessarily perform well out-of-sample, at a collection of sites not used for training. We explore this more below.

25 We use the ensemble dependence transformation process presented in Bishop and Abramowitz (2013) to calculate the spatiotemporal uncertainty of DOLCE. This involves first quantifying the discrepancy between our weighted ET estimate, μ_e, and the flux tower data, expressed as an error variance, s_e^2, over time and space. We then transform our Diagnostic Ensemble so that its variance about μ_e at a given time-space step, σ_e^{2j}, averaged over all time and space steps where we have flux tower data, is equal to s_e^2. This process ensures that the spread of the transformed Diagnostic Ensemble provides a better

uncertainty estimate than simply using the spread of all products in the original Diagnostic Ensemble, since the spread of the transformed ensemble now accurately reflects uncertainty in those grid cells where flux tower data is available.

We calculate the discrepancy between observations and our weighted mean as

$$s_e^2 = \frac{\sum_{j=1}^{J}(\mu_e^j - y^j)^2}{J-1} \tag{2}$$

5 Next, we wish to ensure that

$$\frac{1}{J}\sum_{j=1}^{J} \sigma_e^{2j} = s_e^2 \tag{3}$$

but the variance of our existing Diagnostic Ensemble will not, in general, satisfy this equation. To transform it so that it does, we first modify the coefficients from Eq. (1), so that they're guaranteed to all be positive:

$$\widetilde{w} = \frac{w^T + (\alpha-1)\frac{1^T}{K}}{\alpha} \tag{4}$$

10 where $\alpha = 1 - K\min(w_k)$ and $\min(w_k)$ is the smallest negative weight (and α is set 1 if all w_k are non-negative). We then transform the ensemble using

$$\tilde{x}_k^j = \mu_e^j + \beta(\bar{x}^j + \alpha(x_k^j - \bar{x}^j) - \mu_e^j) \tag{5}$$

where

$$\beta = \sqrt{\frac{s_e^2}{\frac{1}{J}\sum_{j=1}^{J}\sum_{k=1}^{K}\widetilde{w}_k(\bar{x}^j + \alpha(x_k^j - \bar{x}^j) - \mu_e^j)^2}} \tag{6}$$

15 If we then define the weighted variance estimate

$$\sigma_e^{2j} = \sum_{k=1}^{K}\widetilde{w}_k(\tilde{x}_k^j - \mu_e^j)^2 \tag{7}$$

we ensure that both Eq. (3) above holds, and also that $\mu_e^j = \sum_{k=1}^{K} w_k x_k^j = \sum_{k=1}^{K} \widetilde{w}_k \tilde{x}_k^j$ (see Bishop and Abramowitz, 2013, for proofs). We then use $\sqrt{\sigma_e^{2j}}$ as the spatially and temporally varying estimate of uncertainty standard deviation, which we will refer to below as Uncertainty SD.

20 **2.4 Experimental setup**

We employed three statistical metrics that reflect how well a gridded ET product represents the quality controlled flux tower observations: Mean Square Error MSE=mean(dataset - observation)^2; Relative Standard Deviation RSD $= |\frac{\sigma_{dataset}}{mean_{dataset}} - \frac{\sigma_{observation}}{mean_{observation}}|$ and Correlation COR=corr(observation, dataset)

In every test, we split the available sites into in-sample and out-of-sample sites (that is, calibration and validation sites).

25 First, we applied the weighting process at the in-sample sites to weight the individual datasets of the Diagnostic Ensemble and derive a weighted product. Then, we calculated the three metrics above using the out-of-sample sites and displayed results by showing:

a.   The percentage performance improvement of the derived weighted product compared to the equally weighted mean (Wmean) of the Diagnostic Ensemble;

b.   The percentage performance improvement of the derived weighted product compared to each individual product in the Reference Ensemble, yielding 10 different values of performance improvement.

5   c.   The aggregate (Ragg) of the values of performance improvement calculated across all 10 products in the Reference Ensemble.

We first divide sites between the in-sample and out-of-sample groups by randomly selecting 25 % of the sites as out-of-sample. The remaining sites form the in-sample training set and are used to calculate a scalar bias correction term and a
10   weight for each participating gridded ET product. These bias correction terms and the weights are then applied to the products at the out-of-sample sites. The test was repeated 5000 times with different random selection of sites being out of sample.

Next, we repeat the process with just one site in the out-of-sample testing group. The bias corrections and weights are therefore derived on all sites except one, and tested on the single out-of-sample site. The same test was repeated for all the
15   participating sites.

3. Results

The results for the 25 % out-of-sample test are displayed in the box and whisker plots presented in Fig. 3 (a), (b) and (c). The MSE plot in Fig. 3a indicates that across most of the random selections of the 25 % out-of-sample sites, the MSE of the weighted product is better than the ensemble mean. The weighting improved results for almost all random selections of sites
20   when compared to each individual dataset in the Reference Ensemble. The RSD plot (Fig. 3b) shows that the weighting succeeded in improving RSD relative to the equally weighted mean (Wmean) of the Diagnostic Ensemble and most of the products in the reference ensemble across almost all the combinations of sites but didn't improve RSD relative to GLEAM-V2B and CSIRO. This is perhaps unsurprising, given that both the weighted and unweighted mean should have decreased variability when the variations in individual products are not temporally coincident. The COR plot (Fig. 3 (c)) shows that
25   despite the expected drop in variability in the weighted product, the correlation with site data has in fact improved across most of the different random selections of the 25 % out-of-sample sites, relative to all of the Reference Ensemble datasets. The improvement was minimal relative to Wmean and MPI.

The results of the one site out-of-sample tests are displayed in Fig. 4 (a), (b) and (c). These box plots indicate that across all
30   the metrics the weighted mean outperformed all the products in the Reference Ensemble. However, when the performance improvement of the weighted product is compared against Wmean the results were inconclusive. In MSE, an improvement

was achieved at more than half of the sites (Fig. 4 (a)). In RSD, as many showed improvement as those that didn't (Fig. 4 (b)) Finally in COR, at more than half of the sites the performance decreased (Fig. 4 (c)).

The results of the one site out-of-sample test suggest that spatial heterogeneity - the discrepancy between site and grid scale estimates, is significant, as the spread of these box plots is large. These sites are more likely to be where the fetch of the flux site observations cannot represent the data of the entire grid (estimates). A further analysis (not shown here) has indicated that sites that show poor improvement in Fig. 4 (a), (b) and (c) have a consistently high bias against all of the gridded products.

To investigate the effect this spatial heterogeneity is having on the out-of-sample tests, we also repeat the one site out-of-sample experiments using a subset of the sites within grid cells that are deemed to be relatively homogeneous (Fig. 4 (d), (e) and (f)). Homogeneity is defined in this case by using only those sites that have the same IGBP vegetation type as the grid cell that contains them. Almost all the gridded ET products use the dominant land cover type for computing ET, yet this is not always the same as the land cover type surrounding the flux site. Since this mismatch occurs in heterogeneous terrains, we will denote the sites that have this property as "HET" sites, whereas the sites that show agreement with the underlying grid cell vegetation type we denoted as "HOM" sites. We retrieve the IGBP vegetation cover data of the grid cells from MODIS Land Cover for year 2009 at 0.5° spatial resolution (Channan et al., 2014, http://glcf.umd.edu/data/lc/; Friedl et al., 2010). The vegetation type of individual sites is taken from metadata on the FLUXNET website. There is some expectation that DOLCE will show better performance at HOM sites compared to HET sites, although HET sites consist of about two-thirds of the total number of sites used in this study. To further investigate this idea, we carried out the one site out-of-sample test training and testing on HOM sites data only. Figures 4 (d), (e) and (f) show that the HOM subset of tower sites does indeed improve the result at least in terms of MSE and COR when compared to the original dataset (HOM & HET; Fig. 4 (a), (b) and (c)). We did not investigate the 25 % out-of-sample tests with HOM sites, since the number of in-sample sites would become too small, and likely lead to overfitting.

On the basis of the widespread out-of-sample improvement that this approach offers over existing gridded ET products, in terms of MSE, RSD and COR against site data, we now present details of the DOLCE product, which is trained using all site data.

We calculated four statistics - Mean Bias, RMSE, Standard Deviation (SD) difference and Correlation - to see how well DOLCE performs at each site. The results are displayed in Fig. 5 (a), (b), (c) and (d). At about 50 % of sites, DOLCE had values between –6 and 6 W m^{-2}, –5 and 5 W m^{-2} in the Mean bias and SD difference metrics respectively, and values greater than 0.93 W m^{-2} and less than 14 W m^{-2} in correlation and RMSE respectively. DOLCE metrics vary in the range [–43.4–30.1 W m^{-2}] for mean bias, [–25.8–23.5 W m^{-2}] for SD difference, [0.09–0.99 W m^{-2}] for correlation and [4.2–60.9 W m^{-2}] for RMSE.

We also calculate the on-site metrics (i.e., RMSE, Mean Bias, SD difference, and Correlation) for DOLCE separately for each subset of sites (i.e. HOM and HET) and we displayed the results in two boxplots (Fig. 5 (left column)). These boxplots show that most of the sites at which DOLCE showed low performance are HET sites.

We calculated the global mean ET for the three DOLCE tiers and for DOLCE (composite of DOLCE tiers as shown in Fig. 1) from 120 monthly means between 2000 and 2009 (Table 2). The computed values vary significantly across the three tiers. The differences in the global monthly means across DOLCE and the three tiers result from the different spatial coverage of the three tiers.

5 We now look at the differences between DOLCE and two widely used ET products. Figure 6 shows the seasonal mean difference ET between MPIBGC and DOLCE and between LandFlux-EVAL-DIAG and DOLCE (Fig. 7). The differences were computed from seasonal means using the same mask over the period 2000–2009 for MPIBGC and 2000–2005 for LandFlux-EVAL-DIAG. The seasonal plots in Fig. 6 show that overall DOLCE has lower ET than MPIBGC. DOLCE tends to have higher ET values in the Asian and Australian tropics during the austral summer and autumn. DOLCE has higher ET

10 values in Sahel during Sep–Nov and in the high plateau of Madagascar during Dec–May. In the Amazon, DOLCE exhibits higher ET values between June and November. Higher values of DOLCE are seen in Guiana highlands throughout the year. The Brazilian highlands show higher values for MPIBGC from June to November. The Mid latitudes of the Northern hemisphere show higher values for MPIBGC between March and August but no significant differences are seen in this area between September and February.

15 In Fig. 7, there are large differences in ET showing higher values in LandFlux-EVAL-DIAG ET over the Amazon, the Rainforests of Southeast Asia and in the high plateau of Madagascar throughout the year. DOLCE tends to exhibit higher ET values in the Ethiopian highlands and Myanmar between June and November.

The spatial distribution of DOLCE mean ET and uncertainty over the austral Summer (Dec–Feb) and Winter (Jun–Aug) from 2000 to 2009 is shown in Fig. 8 (a) and (b) respectively. The magnitude of the seasonal change of ET is minor in the

20 tropical regions over the Congo basin, the South-eastern part of the Brasilian highlands, the Ethiopian Highland and Southeast Asia. ET doesn't exhibit any seasonal change over Greenland and the deserts in North Africa (Sahara), the middle east (Arabian Peninsula desert) and Asia (i.e. Gobi, Takla Makan and Thar). Figure 8 (c) is intended to give some indication of the reliability of DOLCE. Regions in blue show grid cells that satisfy $\frac{\text{Uncertainty SD}}{\text{mean ET}} \leq 1$. Those shown in green have $|\text{mean ET}|<5$ and Uncertainty SD < 10 but don't satisfy $\frac{\text{Uncertainty SD}}{\text{mean ET}} \leq 1$, so that the uncertainty estimates are higher than

25 their associated ET, but both the uncertainty and the ET estimates are very small. All the remaining grid cells, perhaps those least reliable, are shown in red. The global maps in Fig. 8 (c) shows that most of the non-reliable uncertainty values are located in the land added in tier 3 (Fig. 2 in yellow). This is not surprising, because uncertainty values have been derived using only two gridded ET datasets that are also not observationally constrained due to the lack of the sites representing the terrestrial ecosystems and environmental conditions in these areas. Some regions show unreliable uncertainty estimates

30 during the cold season only, located in the plateau of Tibet, over the Andes, the Australian deserts, the South-African deserts, American Great basin and Rocky Mountains.

4. Discussion

The results of the one site out-of-sample and 25 % out-of-sample tests above suggest that the weighting of gridded ET products in this way produces a more capable ET product overall. Critically, the fact that the weighting improves out of sample performance suggests that while the representativeness of point-scale measurement for the grid scale may not exist at
5   every single site, it does exist across all these sites as a whole.

It might be reasonable to assume that eliminating sites that poorly represent grid cell properties might further improve these results, yet the results of categorizing sites into HOM and HET subsets suggested that this is not necessarily a simple process. Our characterisation was based on a relatively simple vegetation characterisation, yet there are a range of soil-vegetation interactions that likely affect ET in each location that are not captured in this classification. Among HET sites, for
10   example, the worst performance occurred at AU-Fog. This poor performance is a reflection of the large discrepancy between the land cover seen by the flux tower which is a wetland landscape in a monsoonal climate, and thus characterised by high evaporation rates throughout the year and the Savannah land cover seen by the satellite products where the vegetation dries or dies in the dry season. Also, we note that none of the six diagnostic products was able to reproduce the flux measured at this site. Perhaps unsurprisingly, DOLCE scored the worst values for Correlation, RMSE and Mean Bias in
15   AU-Fog.

Aside from AU-Fog, three sites showed low correlation (less than 0.5) between DOLCE and observations. These include ID-Pag, ES-LgS and IL-Yat (see Supplementary Table S1). IL-Yat site is an Evergreen Needleleaf Forest site located over a desert (Bare) grid cell and therefore belongs to the HET case which might be the reason for the discrepancy between the satellite derived ET and the observed ET. ID-Pag belongs to the HOM case, but a burning event occurred in a nearby forest
20   between mid-August and late October, 2002 and caused the site to be covered with a dense smoke-haze. Although these three months were excluded from the analysis, it is very likely that the burned region produced extremely different ET compared to the surrounding unburned landscape, making it a HET site until the regeneration of the vegetation and might be the reason why the weighting products couldn't reproduce ET in the following couple of months. ES-LgS is an Open Shrubland site that belongs to the HOM case. This site operated from 2007 to 2009 and is currently inactive. The reason of
25   the low correlation of DOLCE with the observed fluxes is not clear, however previous studies (Ershadi et al., 2014; McCabe et al., 2016) stated that the complexity of shrubland landscape is the cause of the poor performance of many models (PM, GLEAM and PT–JPL). In the case of DOLCE, the poor performance was revealed in one metric only (i.e. correlation).

These results nevertheless lead us to expect that if we construct DOLCE by incorporating homogeneous sites only, we might get a better product, but the small number of sites satisfying this property, and the difficulty in defining a meaningful
30   definition for expected flux homogeneity are limiting factors.

Figure 9 shows that DOLCE performs differently for different vegetation types, at least as sampled by the flux towers we use here. Previous studies have shown that different ET estimation approaches perform differently over different biomes. For example, Ershadi et al. (2014) found that the PM models outperform PT–JPL across grasslands, croplands and deciduous

broadleaf forest, but PT–JPL has higher performance than PM models over shrublands and evergreen needleleaf forest biomes. McCabe et al. (2016) observed poor performance of GLEAM, PM models and PT–JPL over shrublands and low performance over the forest biomes and higher performance over short canopies. The number of sites for each vegetation type in our case varies, with four for Open Shrublands (OSH), 39 for evergreen needleleaf forest (ENF), nine for evergreen

5   broadleaf forests (EBF), 18 for deciduous broadleaf Forest (DBF), 10 for Mixed Forests (MF), four for Woody Savannas (WSA), four for Savannas (SAV), 42 for grassland (GRA), eight for Wetland (WET), one for Cropland/Natural Vegetation Mosaic (VEG) and 19 for Croplands (CRO). Of the 159 sites that are used to weight the tier 3 products (GLEAM v2A and GLEAM v3A), only 142 sites are within the spatial coverage of DOLCE. This decrease is caused by the coarser resolution of DOLCE compared to GLEAM products. The remaining 17 sites were located on grids that were identified as land grid cells

10   in GLEAM's spatial resolution (0.25º) but water body in DOLCE's spatial resolution (0.5º). We additionally tried to cluster flux tower sites into groups (such as vegetation type) so that each group maintains enough members to allow the in- and out-of-sample testing approach used above. We tried clustering by vegetation type, climate zone and aridity index, and implemented the same one site out-of-sample testing approach as above. The motivation for this approach was to try to reduce the number of sites that did not show improvement as a result of the weighting, and ideally improve performance of

15   DOLCE overall, yet none of these clustering approaches delivered any improvement, possibly due to the considerably reduced sample size in each cluster (increasing the likelihood of overfitting). It might also be a result of grid cell heterogeneity within the small sample that constitutes each vegetation type. Finally, as noted above, we have no guarantee that vegetation type is necessarily a good proxy for surface flux behaviour. A summary of this investigation is included in the supplementary material.

20   In this study, DOLCE was derived by combining remote sensing products that use an empirical approach (i.e. MPIBGC) and a more physical approach (i.e. MOD16, GLEAM v2A, GLEAM v2B and GLEAM v3A and PML). Constructing an ET product by combining different approaches can take advantage of their desirable features and reduce their limitations (Zhang et al., 2016). This is indeed reflected by the enhanced performance of DOLCE over all the biome types against the reference products. Table 3 shows that the weights were attributed almost equally to each approach (i.e. ≈ 0.5 for both MPIBGC and

25   the physical ensemble in tier 1 and tier 2), which indicates that the two approaches contributed equally in deriving DOLCE. It is important to mention that the weighting approach offers the possibility of enhancing DOLCE in the future by incorporating any ET dataset that becomes available (for example, HOLAPS v1.0, Loew et al., 2016).

The limitations of the weighting approach presented here arise from issues in the observational data and limitations in the weighted datasets that are employed. FLUXNET data inevitably has some instrumentation-related problems (Göckede et al.,

30   2008) that affect the data quality of the measured flux in some terrains and under some environmental conditions. Moreover, FLUXNET sites are not globally-representative of all terrestrial ecosystems, and not evenly distributed across the biome types, which might lead to biases when computing the weights of the products in favour of the product that outperforms over the most frequent cover types. Also, in some areas where tower density is relatively high, the information from different towers is not necessarily independent.

Finally, a common imperfection in all the weighted products due to for example anthropogenic water management, will of course lead to the same imperfection in the derived product.

The uncertainty estimate presented here is firmly grounded in the spread of existing gridded ET products, but is better than this spread alone, since this spread has been recalibrated so that the uncertainty of DOLCE where flux tower data exists is precisely the spread of the recalibrated products.

5 Conclusion

In this study, we presented a new global ET product with monthly temporal resolution for 2000–2009 at 0.5° spatial resolution and a calibrated estimate of its uncertainty. The approach used to weight existing gridded ET products accounted for both the performance differences and error covariance between the participating ET products. The DOLCE product performs better than any of its six constituent members overall, as well outperforming other well-known gridded ET products (CSIRO, LandFlux-EVAL-ALL, LandFlux-EVAL-DIAG and PT–JPL) across a range of metrics. It was shown that despite the scale mismatch between the flux tower and the grid cell, the ensemble of flux towers as a whole can provide information about the grid cells that contain them. While the representativeness of the point scale for the grid scale is enhanced by only considering sites that lie within homogeneous grid cells we suggest that an optimal definition of homogeneity for flux behaviour be the subject of future investigation. Nevertheless, DOLCE appears to outperform existing gridded ET products overall, and offers the opportunity for improvement as more flux tower data and new gridded ET products become available.

6 Competing interests

The authors declare that they have no conflict of interest.

7 Data availability

DOLCE v1.0 can be downloaded from geonetwork.nci.org.au and its DOI is http://dx.doi.org/10.4225/41/58980b55b0495

8 Acknowledgements

We acknowledge the support of the Australian Research Council Centre of Excellence for Climate System Science (CE110001028). This work used eddy covariance data acquired and shared by the FLUXNET community, including these networks: AmeriFlux, AfriFlux, AsiaFlux, CarboAfrica, CarboEuropeIP, CarboItaly, CarboMont, ChinaFlux, Fluxnet-Canada, GreenGrass, ICOS, KoFlux, LBA, NECC, OzFlux-TERN, TCOS-Siberia, and USCCC. The ERA-Interim reanalysis data are provided by ECMWF and processed by LSCE. The FLUXNET eddy covariance data processing and

harmonization was carried out by the European Fluxes Database Cluster, AmeriFlux Management Project, and Fluxdata project of FLUXNET, with the support of CDIAC and ICOS Ecosystem Thematic Center, and the OzFlux, ChinaFlux and AsiaFlux offices. This work also used eddy covariance data acquired by the FLUXNET community and in particular by the following networks: AmeriFlux (U.S. Department of Energy, Biological and Environmental Research, Terrestrial Carbon

5   Program (DE - FG02 - 04ER63917 and DE-FG02 - 04ER63911)), AfriFlux, AsiaFlux, CarboAfrica, CarboEuropeIP, CarboItaly, CarboMont, ChinaFlux, Fluxnet - Canada (supported by CFCAS, NSERC, BIOCAP, Environment Canada, and NRCan), GreenGrass, KoFlux, LBA, NECC, OzFlux, TCOS - Siberia, USCCC. We acknowledge the financial support to the eddy covariance data harmonization provided by CarboEuropeIP, FAO - GTOS - TCO, iLEAPS, Max Planck Institute for Biogeochemistry, National Science Foundation, University of Tuscia, Université Laval and Environment Canada and US

10 Department of Energy and the database development and technical support from Berkeley Water Center, Lawrence Berkeley National Laboratory, Microsoft Research eScience, Oak Ridge National Laboratory, University of California - Berkeley, University of Virginia.

9 References

Abramowitz, G.: Towards a benchmark for land surface models, Geophys. Res. Lett., 32(22), n/a-n/a,
15 doi:10.1029/2005GL024419, 2005.

Abramowitz, G.: Towards a public, standardized, diagnostic benchmarking system for land surface models, Geosci. Model Dev., 5(3), 819–827, doi:10.5194/gmd-5-819-2012, 2012.

Annan, J. D. and Hargreaves, J. C.: Reliability of the CMIP3 ensemble, Geophys. Res. Lett., 37(2), n/a-n/a, doi:10.1029/2009GL041994, 2010.

20 Badgley, G., Fisher, J. B., Jiménez, C., Tu, K. P., Vinukollu, R., Badgley, G., Fisher, J. B., Jiménez, C., Tu, K. P. and Vinukollu, R.: On Uncertainty in Global Terrestrial Evapotranspiration Estimates from Choice of Input Forcing Datasets*, J. Hydrometeorol., 16(4), 1449–1455, doi:10.1175/JHM-D-14-0040.1, 2015.

Baldocchi, D.: "Breathing" of the terrestrial biosphere: lessons learned from a global network of carbon dioxide flux measurement systems, Aust. J. Bot., 56(1), 1, doi:10.1071/BT07151, 2008.

25 Baldocchi, D., Falge, E., Gu, L., Olson, R., Hollinger, D., Running, S., Anthoni, P., Bernhofer, C., Davis, K., Evans, R., Fuentes, J., Goldstein, A., Katul, G., Law, B., Lee, X., Malhi, Y., Meyers, T., Munger, W., Oechel, W., Paw, K. T., Pilegaard, K., Schmid, H. P., Valentini, R., Verma, S., Vesala, T., Wilson, K., Wofsy, S., Baldocchi, D., Falge, E., Gu, L., Olson, R., Hollinger, D., Running, S., Anthoni, P., Bernhofer, C., Davis, K., Evans, R., Fuentes, J., Goldstein, A., Katul, G., Law, B., Lee, X., Malhi, Y., Meyers, T., Munger, W., Oechel, W., Paw, K. T., Pilegaard, K., Schmid, H. P., Valentini, R.,

30 Verma, S., Vesala, T., Wilson, K. and Wofsy, S.: FLUXNET: A New Tool to Study the Temporal and Spatial Variability of Ecosystem–Scale Carbon Dioxide, Water Vapor, and Energy Flux Densities, Bull. Am. Meteorol. Soc., 82(11), 2415–2434, doi:10.1175/1520-0477(2001)082<2415:FANTTS>2.3.CO;2, 2001.

Belelli Marchesini, L., Papale, D., Reichstein, M., Vuichard, N., Tchebakova, N. and Valentini, R.: Carbon balance assessment of a natural steppe of southern Siberia by multiple constraint approach, Biogeosciences, 4, 581–595 [online] Available from: www.biogeosciences.net/4/581/2007/ (Accessed 13 March 2017), 2007.

Best, M. J., Abramowitz, G., Johnson, H. R., Pitman, A. J., Balsamo, G., Boone, A., Cuntz, M., Decharme, B., Dirmeyer, P. A., Dong, J., Ek, M., Guo, Z., Haverd, V., van den Hurk, B. J. J., Nearing, G. S., Pak, B., Peters-Lidard, C., Santanello, J. A., Stevens, L., Vuichard, N., Best, M. J., Abramowitz, G., Johnson, H. R., Pitman, A. J., Balsamo, G., Boone, A., Cuntz, M., Decharme, B., Dirmeyer, P. A., Dong, J., Ek, M., Guo, Z., Haverd, V., Hurk, B. J. J. van den, Nearing, G. S., Pak, B., Peters-Lidard, C., Jr., J. A. S., Stevens, L., Vuichard, N., J Van Den Hurk, B. J., Nearing, G. S., Pak, B., Peters-Lidard, C., Santanello Jr, J. A., Stevens, L. and Vuichard, N.: The Plumbing of Land Surface Models: Benchmarking Model Performance, J. Hydrometeorol., 16(3), 1425–1442, doi:10.1175/JHM-D-14-0158.1, 2015.

Bishop, C. H. and Abramowitz, G.: Climate model dependence and the replicate Earth paradigm, Clim. Dyn., doi:10.1007/s00382-012-1610-y, 2013.

Bowen, I. S.: The Ratio of Heat Losses by Conduction and by Evaporation from any Water Surface, Phys. Rev., 27(6), 779–787, doi:10.1103/PhysRev.27.779, 1926.

Brutsaert, W. and Stricker, H.: An advection-aridity approach to estimate actual regional evapotranspiration, Water Resour. Res., 15(2), 443–450, doi:10.1029/WR015i002p00443, 1979.

Burba, G. and Anderson, D.: Eddy Covariance Flux Measurements, Ecol. Appl., 18(6), 211 [online] Available from: http://www.ncbi.nlm.nih.gov/pubmed/18767616, 2010.

Channan, S., Collins, k. and Emanuel, W. R.: Global mosaics of the standard MODIS land cover type data, University of Maryland and the Pacific Northwest National Laboratory, College Park, Maryland, USA, 2014

Chen, T. H., Henderson-Sellers, A., Milly, P. C. D., Pitman, A. J., Beljaars, A. C. M., Polcher, J., Abramopoulos, F., Boone, A., Chang, S., Chen, F., Dai, Y., Desborough, C. E., Dickinson, R. E., Dümenil, L., Ek, M., Garratt, J. R., Gedney, N., Gusev, Y. M., Kim, J., Koster, R., Kowalczyk, E. A., Laval, K., Lean, J., Lettenmaier, D., Liang, X., Mahfouf, J.-F., Mengelkamp, H.-T., Mitchell, K., Nasonova, O. N., Noilhan, J., Robock, A., Rosenzweig, C., Schaake, J., Schlosser, C. A., Schulz, J.-P., Shao, Y., Shmakin, A. B., Verseghy, D. L., Wetzel, P., Wood, E. F., Xue, Y., Yang, Z.-L., Zeng, Q., Chen, T. H., Henderson-Sellers, A., Milly, P. C. D., Pitman, A. J., Beljaars, A. C. M., Polcher, J., Abramopoulos, F., Boone, A., Chang, S., Chen, F., Dai, Y., Desborough, C. E., Dickinson, R. E., Dümenil, L., Ek, M., Garratt, J. R., Gedney, N., Gusev, Y. M., Kim, J., Koster, R., Kowalczyk, E. A., Laval, K., Lean, J., Lettenmaier, D., Liang, X., Mahfouf, J.-F., Mengelkamp, H.-T., Mitchell, K., Nasonova, O. N., Noilhan, J., Robock, A., Rosenzweig, C., Schaake, J., Schlosser, C. A., Schulz, J.-P., Shao, Y., Shmakin, A. B., Verseghy, D. L., Wetzel, P., Wood, E. F., Xue, Y., Yang, Z.-L. and Zeng, Q.: Cabauw Experimental Results from the Project for Intercomparison of Land-Surface Parameterization Schemes, J. Clim., 10(6), 1194–1215, doi:10.1175/1520-0442(1997)010<1194:CERFTP>2.0.CO;2, 1997.

Ershadi, A., McCabe, M. F., Evans, J. P., Chaney, N. W. and Wood, E. F.: Multi-site evaluation of terrestrial evaporation models using FLUXNET data, Agric. For. Meteorol., doi:10.1016/j.agrformet.2013.11.008, 2014.

Fisher, J. B., Tu, K. P. and Baldocchi, D. D.: Global estimates of the land-atmosphere water flux based on monthly AVHRR and ISLSCP-II data, validated at 16 FLUXNET sites, Remote Sens. Environ., doi:10.1016/j.rse.2007.06.025, 2008a.

Fisher, J. B., Tu, K. P. and Baldocchi, D. D.: Global estimates of the land-atmosphere water flux based on monthly AVHRR and ISLSCP-II data, validated at 16 FLUXNET sites, Remote Sens. Environ., 112(3), 901–919, doi:10.1016/j.rse.2007.06.025, 2008b.

Friedl, M. A., Sulla-Menashe, D., Tan, B., Schneider, A., Ramankutty, N., Sibley, A. and Huang, X.: MODIS Collection 5 global land cover: Algorithm refinements and characterization of new datasets, Remote Sens. Environ., 114, 168–182, doi:10.1016/j.rse.2009.08.016, 2010.

Göckede, M., Foken, T., Aubinet, M., Aurela, M., Banza, J., Bernhofer, C., Bonnefond, J. M., Brunet, Y., Carrara, A., Clement, R., Dellwik, E., Elbers, J., Eugster, W., Fuhrer, J., Granier, A., Grünwald, T., Heinesch, B., Janssens, I. A., Knohl, A., Koeble, R., Laurila, T., Longdoz, B., Manca, G., Marek, M., Markkanen, T., Mateus, J., Matteucci, G., Mauder, M., Migliavacca, M., Minerbi, S., Moncrieff, J., Montagnani, L., Moors, E., Ourcival, J.-M., Papale, D., Pereira, J., Pilegaard, K., Pita, G., Rambal, S., Rebmann, C., Rodrigues, A., Rotenberg, E., Sanz, M. J., Sedlak, P., Seufert, G., Siebicke, L., Soussana, J. F., Valentini, R., Vesala, T., Verbeeck, H. and Yakir, D.: Quality control of CarboEurope flux data–Part 1: Coupling footprint analyses with flux data quality assessment to evaluate sites in forest ecosystems, Biogeosciences, 5(2), 433–450, doi:10.5194/bg-5-433-2008, 2008.

Haughton, N., Abramowitz, G., Pitman, A. J., Or, D., Best, M. J., Johnson, H. R., Balsamo, G., Boone, A., Cuntz, M., Decharme, B., Dirmeyer, P. A., Dong, J., Ek, M., Guo, Z., Haverd, V., van den Hurk, B. J. J., Nearing, G. S., Pak, B., Santanello, J. A., Stevens, L. E., Vuichard, N., Haughton, N., Abramowitz, G., Pitman, A. J., Or, D., Best, M. J., Johnson, H. R., Balsamo, G., Boone, A., Cuntz, M., Decharme, B., Dirmeyer, P. A., Dong, J., Ek, M., Guo, Z., Haverd, V., Hurk, B. J. J. van den, Nearing, G. S., Pak, B., Jr., J. A. S., Stevens, L. E. and Vuichard, N.: The Plumbing of Land Surface Models: Is Poor Performance a Result of Methodology or Data Quality?, J. Hydrometeorol., 17(6), 1705–1723, doi:10.1175/JHM-D-15-0171.1, 2016.

Jiménez, C., Prigent, C., Mueller, B., Seneviratne, S. I., McCabe, M. F., Wood, E. F., Rossow, W. B., Balsamo, G., Betts, A. K., Dirmeyer, P. A., Fisher, J. B., Jung, M., Kanamitsu, M., Reichle, R. H., Reichstein, M., Rodell, M., Sheffield, J., Tu, K. and Wang, K.: Global intercomparison of 12 land surface heat flux estimates, J. Geophys. Res. Atmos., doi:10.1029/2010JD014545, 2011.

Jung, M., Reichstein, M., Margolis, H. A., Cescatti, A., Richardson, A. D., Arain, M. A., Arneth, A., Bernhofer, C., Bonal, D., Chen, J., Gianelle, D., Gobron, N., Kiely, G., Kutsch, W., Lasslop, G., Law, B. E., Lindroth, A., Merbold, L., Montagnani, L., Moors, E. J., Papale, D., Sottocornola, M., Vaccari, F. and Williams, C.: Global patterns of land-atmosphere fluxes of carbon dioxide, latent heat, and sensible heat derived from eddy covariance, satellite, and meteorological observations, , 116(G3), G00J07, doi:10.1029/2010JG001566, 2011.

Loew, A., Peng, J. and Borsche, M.: High-resolution land surface fluxes from satellite and reanalysis data (HOLAPS v1.0): evaluation and uncertainty assessment, Geosci. Model Dev, 9, 2499–2532, doi:10.5194/gmd-9-2499-2016, 2016.

Martens, B., Miralles, D., Lievens, H., Van Der Schalie, R., De Jeu, R., Fernández-Prieto, D. and Verhoest, N.: GLEAM v3: updated land evaporation and root-zone soil moisture datasets, Geophys. Res. Abstr. EGU Gen. Assem., 18(23), 2016–4253, 2016.

McCabe, M. F., Ershadi, A., Jimenez, C., Miralles, D. G., Michel, D. and Wood, E. F.: The GEWEX LandFlux project: Evaluation of model evaporation using tower-based and globally gridded forcing data, Geosci. Model Dev., doi:10.5194/gmd-9-283-2016, 2016.

Michel, D., Jiménez, C., Miralles, D. G., Jung, M., Hirschi, M., Ershadi, A., Martens, B., McCabe, M. F., Fisher, J. B., Mu, Q., Seneviratne, S. I., Wood, E. F. and Fernández-Prieto, D.: The WACMOS-ET project Part 1: Tower-scale evaluation of four remote-sensing-based evapotranspiration algorithms, Hydrol. Earth Syst. Sci., 20(2), 803–822, doi:10.5194/hess-20-803-2016, 2016.

Miralles, D. G., Holmes, T. R. H., De Jeu, R. A. M., Gash, J. H., Meesters, A. G. C. A. and Dolman, A. J.: Global land-surface evaporation estimated from satellite-based observations, Hydrol. Earth Syst. Sci., 15(2), 453–469, doi:10.5194/hess-15-453-2011, 2011a.

Miralles, D. G., Holmes, T. R. H., De Jeu, R. A. M., Gash, J. H., Meesters, A. G. C. A. and Dolman, A. J.: Global land-surface evaporation estimated from satellite-based observations, Hydrol. Earth Syst. Sci., doi:10.5194/hess-15-453-2011, 2011b.

Monteith, J. L.: Evaporation and environment., Symp. Soc. Exp. Biol., 19, 205–34 [online] Available from: http://www.ncbi.nlm.nih.gov/pubmed/5321565 (Accessed 14 March 2017), 1965.

Mu, Q., Heinsch, F. A., Zhao, M. and Running, S. W.: Development of a global evapotranspiration algorithm based on MODIS and global meteorology data, Remote Sens. Environ., 111(4), 519–536, doi:10.1016/j.rse.2007.04.015, 2007.

Mu, Q., Zhao, M. and Running, S. W.: Improvements to a MODIS global terrestrial evapotranspiration algorithm, Remote Sens. Environ., 115(8), 1781–1800, doi:10.1016/j.rse.2011.02.019, 2011.

Mueller, B., Seneviratne, S. I., Jimenez, C., Corti, T., Hirschi, M., Balsamo, G., Ciais, P., Dirmeyer, P., Fisher, J. B., Guo, Z., Jung, M., Maignan, F., McCabe, M. F., Reichle, R., Reichstein, M., Rodell, M., Sheffield, J., Teuling, A. J., Wang, K., Wood, E. F. and Zhang, Y.: Evaluation of global observations-based evapotranspiration datasets and IPCC AR4 simulations, Geophys. Res. Lett., doi:10.1029/2010GL046230, 2011.

Mueller, B., Hirschi, M., Jimenez, C., Ciais, P., Dirmeyer, P. A., Dolman, A. J., Fisher, J. B., Jung, M., Ludwig, F., Maignan, F., Miralles, D. G., McCabe, M. F., Reichstein, M., Sheffield, J., Wang, K., Wood, E. F., Zhang, Y. and Seneviratne, S. I.: Benchmark products for land evapotranspiration: LandFlux-EVAL multi-data set synthesis, Hydrol. Earth Syst. Sci., doi:10.5194/hess-17-3707-2013, 2013.

Papale, D., Agarwal, D. A., Baldocchi, D., Cook, R. B., Fisher, J. B. and van Ingen, C.: Database Maintenance, Data Sharing Policy, Collaboration, in Eddy Covariance, pp. 399–424, Springer Netherlands, Dordrecht., 2012.

Stöckli, R., Lawrence, D. M., Niu, G.-Y., Oleson, K. W., Thornton, P. E., Yang, Z.-L., Bonan, G. B., Denning, A. S. and Running, S. W.: Use of FLUXNET in the Community Land Model development, J. Geophys. Res. Biogeosciences, 113(G1),

n/a-n/a, doi:10.1029/2007JG000562, 2008.

Su, Z.: The Surface Energy Balance System (SEBS) for estimation of turbulent heat fluxes, Hydrol. Earth Syst. Sci., 6(1), 85–100, doi:10.5194/hess-6-85-2002, 2002.

Sumner, D. M. and Jacobs, J. M.: Utility of Penman–Monteith, Priestley–Taylor, reference evapotranspiration, and pan
5 evaporation methods to estimate pasture evapotranspiration, J. Hydrol., 308(1–4), 81–104, doi:10.1016/j.jhydrol.2004.10.023, 2005.

Twine, T. E., Kustas, W. P., Norman, J. M., Cook, D. R., Houser, P. R., Meyers, T. P., Prueger, J. H., Starks, P. J. and Wesley, M. L.: Correcting eddy-covariance flux underestimates over a grassland, NASA Publ. [online] Available from: http://digitalcommons.unl.edu/nasapub/11 (Accessed 13 March 2017), 2000.

10 Vinukollu, R. K., Wood, E. F., Ferguson, C. R. and Fisher, J. B.: Global estimates of evapotranspiration for climate studies using multi-sensor remote sensing data: Evaluation of three process-based approaches, Remote Sens. Environ., doi:10.1016/j.rse.2010.11.006, 2011.

Wang, K. and Dickinson, R. E.: A review of global terrestrial evapotranspiration: Observation, modeling, climatology, and climatic variability, Rev. Geophys., doi:10.1029/2011RG000373, 2012.

15 Wang, Y. P., Baldocchi, D., Leuning, R., Falge, E. and Vesala, T.: Estimating parameters in a land-surface model by applying nonlinear inversion to eddy covariance flux measurements from eight FLUXNET sites, Glob. Chang. Biol., 13(3), 652–670, doi:10.1111/j.1365-2486.2006.01225.x, 2007.

Zhang, K., Kimball, J. S., Nemani, R. R. and Running, S. W.: A continuous satellite-derived global record of land surface evapotranspiration from 1983 to 2006, Water Resour. Res., 46(9), n/a-n/a, doi:10.1029/2009WR008800, 2010a.

20 Zhang, K., Kimball, J. S. and Running, S. W.: A review of remote sensing based actual evapotranspiration estimation, , 3(6), 834–853, doi:10.1002/wat2.1168, 2016.

Zhang, Y., Leuning, R., Hutley, L. B., Beringer, J., McHugh, I. and Walker, J. P.: Using long-term water balances to parameterize surface conductances and calculate evaporation at 0.05° spatial resolution, Water Resour. Res., 46(5), n/a-n/a, doi:10.1029/2009WR008716, 2010b.

25 Zhang, Y., Peña-Arancibia, J. L., Mcvicar, T. R., Chiew, F. H. S., Vaze, J., Liu, C., Lu, X., Zheng, H., Wang, Y., Liu, Y. Y., Miralles, D. G. and Pan, M.: Multi-decadal trends in global terrestrial evapotranspiration and its components, Nat. Publ. Gr., 6, 19124, doi:10.1038/srep19124, 2015.

30

Tables

Table1: Gridded ET products used in this paper.

ET product and Reference	Abbreviation	Time period & Spatial Resolution	Forcing data source	Calculation Method(s)
CSIRO-global (Zhang et al., 2010a)	CS	1983–2006 0.5°	Meteorological observations from flux tower distributed across all global biome types Remote sensing inputs	An extended ET product of CSIRO (Zhang et al., 2010b) that covers a global domain NDVI-based PM model PT equation for open water evaporation
GLEAM-V2A (Miralles et al., 2011b)	G2A	2000–2009 0.25°	Remote sensing based observations Gauged based precipitation	PT equation Canopy Interception Model, Soil water module and Stress module
GLEAM-V2B (Miralles et al., 2011b)	G2B	2000–2009 0.25°	Remote sensing based observations	PT equation Canopy Interception Module, Soil water module and Stress module
GLEAM-V3A (Martens et al., 2016)	G3A	2000–2012 0.25°	Satellite based inputs Multi-source precipitation	A revised version of GLEAM V2A in which new satellite-observed geophysical variables have been incorporated and the representation of the surface soil moisture and evaporation has been improved
LandFlux-Eval-Diag (Mueller et al.,	LFD	1989–2005	Simple mean of 5 diagnostic ET datasets	

2011, 2013)		1°		
LandFlux-Eval-All (Mueller et al., 2011, 2013)	LFA		Simple mean of 14 Diagnostic, LSM and Reanalysis datasets.	
MOD16 MODIS global ET products (Mu et al., 2011)	MOD	2000–2014 1°	Global Modeling and Assimilation Office (GMAO) meteorological reanalysis data Remote sensing inputs from MODIS 8-day retrievals	PM formula (Monteith, 1965)
MPIBGC (Jung et al., 2011)	MPI	1982–2011 1°	FLUXNET data from 253 sites Remote sensing datasets from (SeaWiFS)	Empirical methods: a Model Tree Ensemble (MTE) Machine learning techniques
PML PM-Leuning model (Zhang et al., 2015)	PML	1981–2012 1°	GMAO Reanalysis products	PM Leuning method
PT–JPL (Fisher et al., 2008b)	PT	1984–2006 1°	Meteorological reanalysis data from ISLSCP –II Remote sensing based observations from monthly AVHRR data	PT equation

Table 2: Standard Deviation (SD) and mean over space and time of DOLCE and the weighting products, derived from the monthly means over the time period 2000-2010 (a total of 120 months) and within the spatial coverage intersect of DOLCE monthly land cover across all the months. All the values are rounded to the nearest tenth

	Tier 1 spatial coverage		Tier 2 spatial coverage		Tier 3 spatial coverage		Tier 1, Tier 2 and Tier 3 composite	
Product	SD W m^{-2}	Mean W m^{-2}	SD W m^{-2}	Mean W m^{-2}	SD W m^{-2}	Mean W m^{-2}	SD W m^{-2}	Mean W m^{-2}
DOLCE	8.9	41.7	11.6	34.7	5.7	20.2	6.4	21.0
MOD16	8.0	42.9	11.0	38.8				
MPIBGC	10.1	44.9	12.8	39.4				

GLEAM-v2A	8.1	43.6	10.6	38.4	6	22.5		
GLEAM-v2B	7.6	43						
GLEAM-v3A	7.7	33.7	10	29.3	5.5	16.5		
PML	8.8	44.6	10.4	38				

Table 3: Weights and bias terms assigned to the weighting products in the case of each of the three DOLCE tiers, and the number of flux tower sites used to feed the weighting.

	DOLCE tier 1 138 sites		DOLCE tier 2 151 sites		DOLCE tier 3 159 sites	
Product	weight	mean bias W m^{-2}	weight	mean bias W m^{-2}	weight	mean bias W m^{-2}
MOD16	0.041	3.756	0.05	4.0		
MPIBGC	0.495	3.837	0.537	3.882		
GLEAM −v2A	−0.026	6.180	0.123	6.098	0.44	5.735
GLEAM-v2B	0.192	−3.571				
GLEAM-v3A	0.171	−5.483	0.151	−5.221	0.56	−6.344
PML	0.127	4.982	0.139	4.668		

Figures
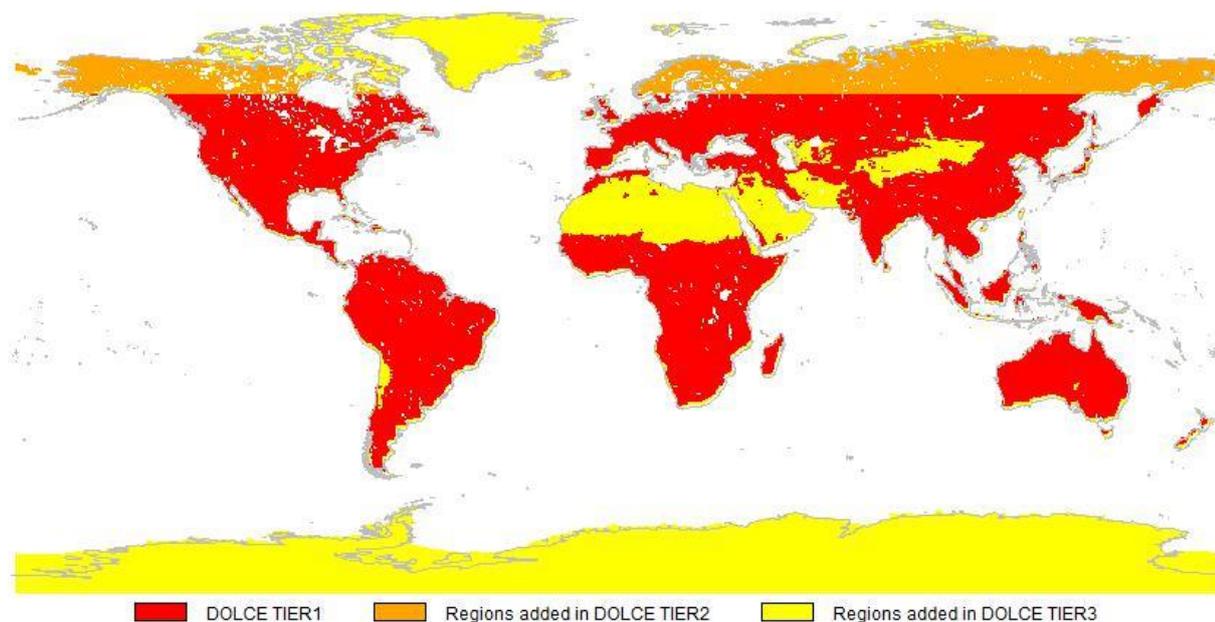
Figure 1: Spatial coverage of DOLCE tier 1 (red), regions added in tier 2 (orange) and tier 3 (yellow). Spatial coverage varies temporally; May 2000 is shown here as a representative example.
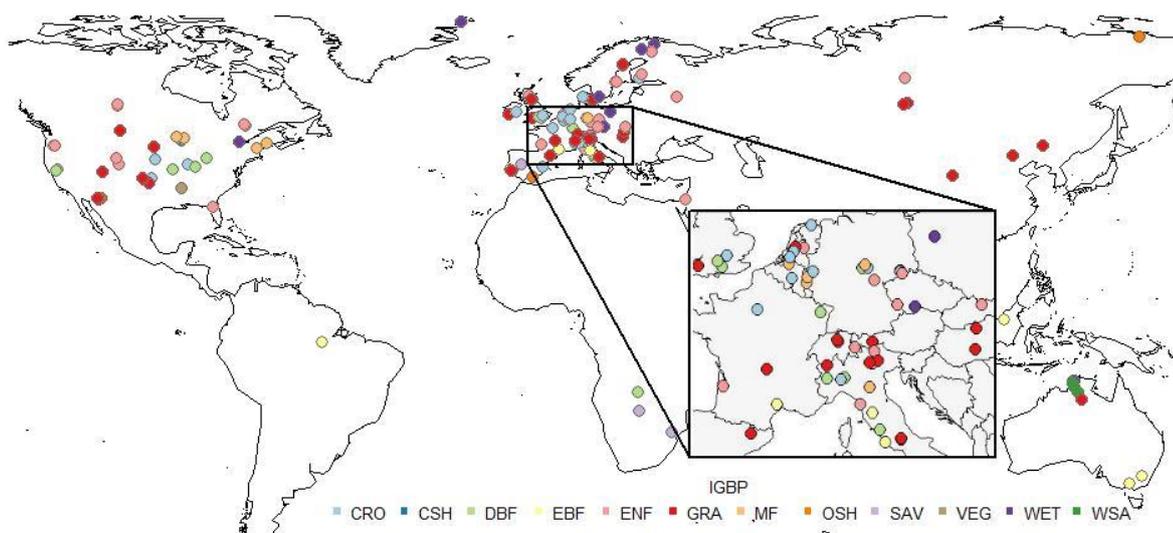
Figure 2: Location of the 159 flux tower sites involved in building DOLCE, classified by vegetation type given by International Geosphere-Biosphere Programme (IGBP): Croplands (CRO), Closed Shrublands (CSH), Deciduous Broadleaf Forest (DBF), Evergreen Broadleaf Forest (EBF), Evergreen Needleleaf Forest (ENF), Grasslands (GRA), Mixed Forests (MF), Open Shrublands (OSH), Savannas (SAV), Cropland/Natural Vegetation mosaic (VEG), Wetlands (WET), and Woody Savannas
10 **(WSA).**
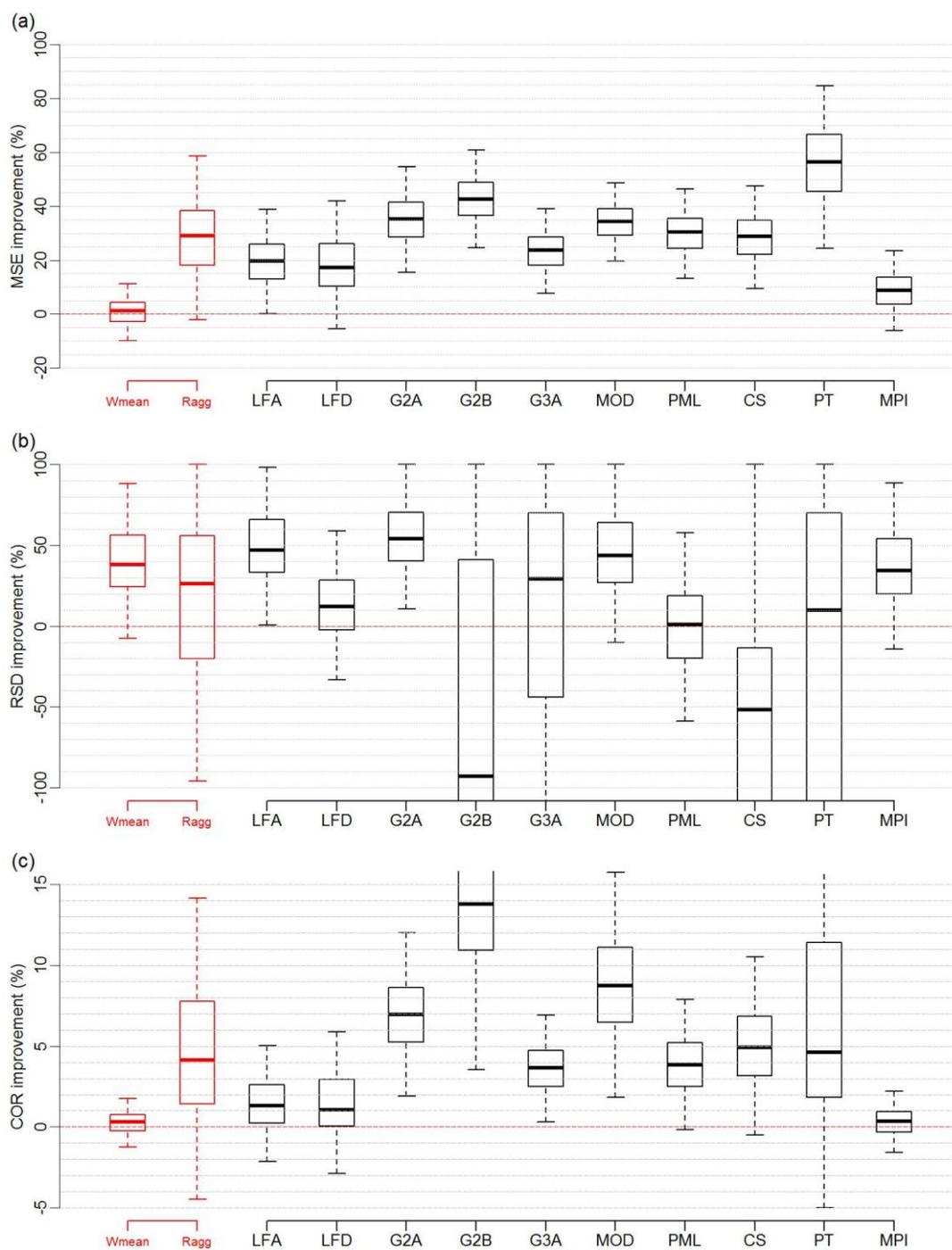
Figure 3: Box and whisker plots displaying the percentage improvement that the weighted product provides in the 25% out-of-sample sites test for three metrics: MSE (a), RSD (b) and COR (c), when compared to equally weighted mean (Wmean) of the Diagnostic Ensemble, aggregated Reference Ensemble (Ragg) and each member of the reference ensemble. Box and whisker plots are generated through randomly selecting the 25% of sites to be out sample 5000 times.
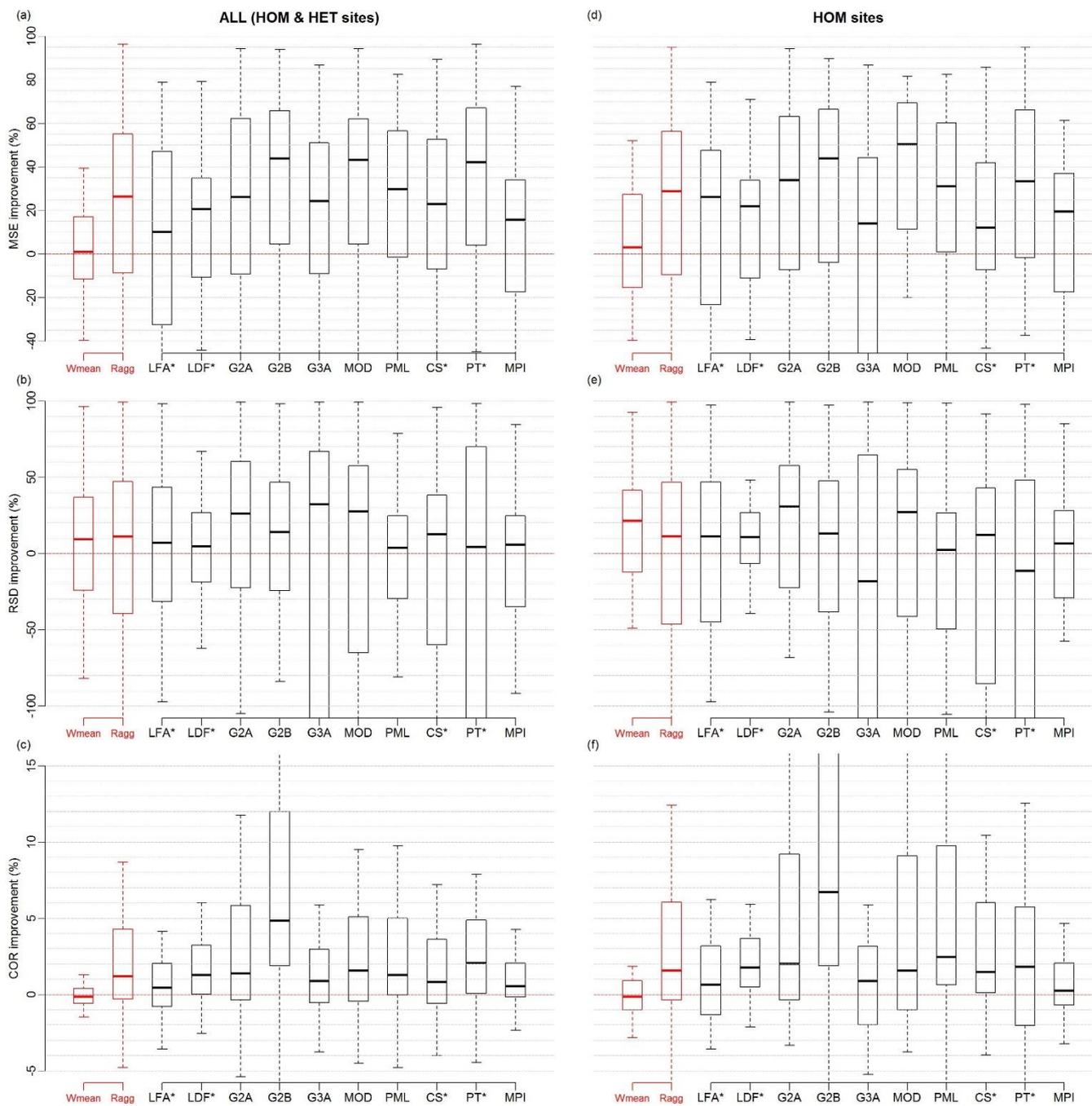
Figure 4: In (a), (b) and (c), as for Fig. 3 but showing the one site out-of-sample tests. Box and whisker plots are generated through selecting one site to be out sample and are repeated for all 138 sites. Testing against the LFA, LFD, CS and PT products was limited to 110, 108, 108 and 72 sites respectively due to the limited spatiotemporal availability of these products relative to the
5 **Diagnostic Ensemble. In (d), (e) and (f), the one out-of-sample test is trained by HOM sites data only.**
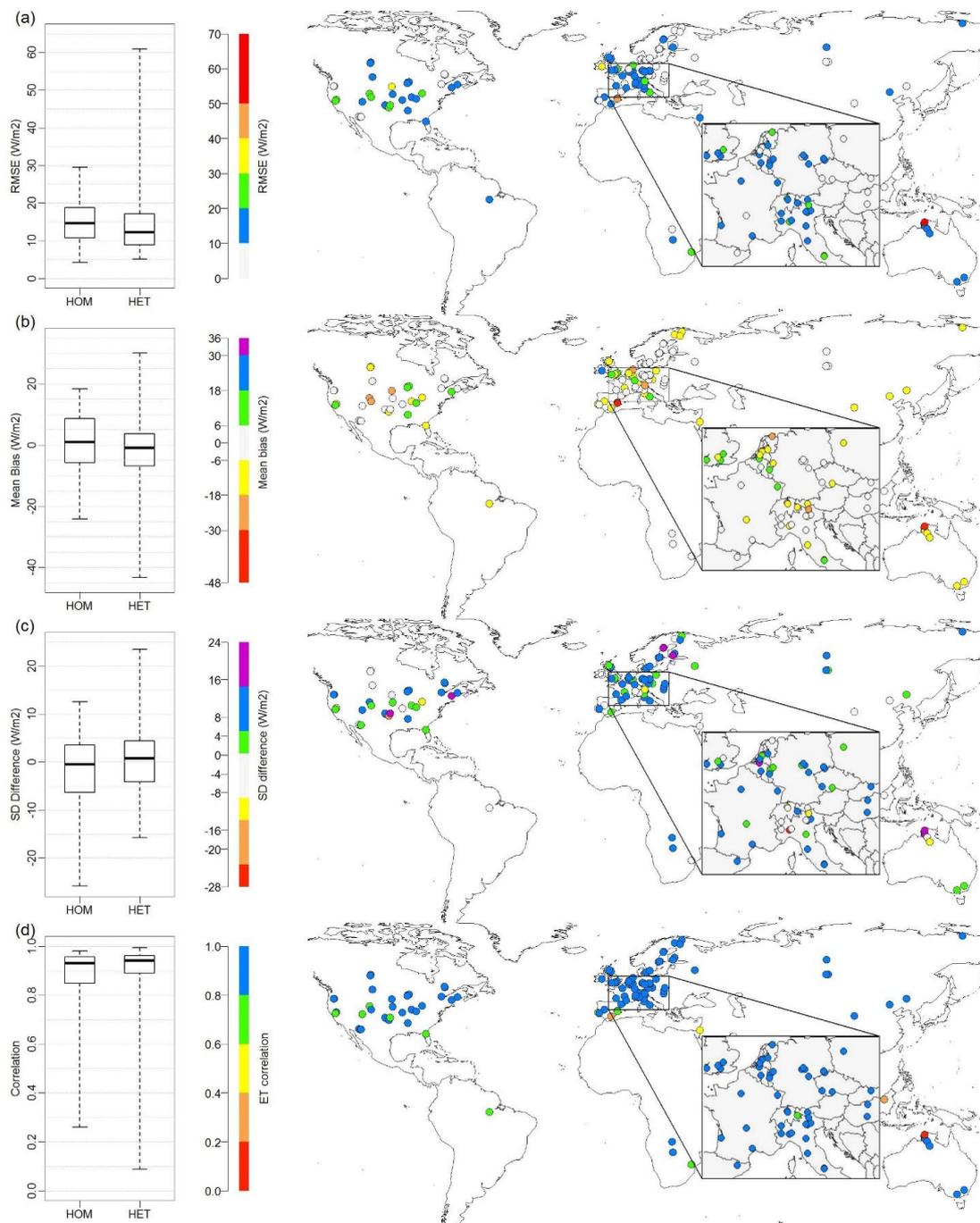
Figure 5: The global maps in the right column show the performance of DOLCE against in-situ measurements at each of the 142 sites by calculating four statistics: (a) RMSE, (b) Mean bias, (c) SD difference and (d) Correlation. The boxplots on the left display the results of these four metrics calculated separately for the sites that are satisfying the HOM case and the HET case.
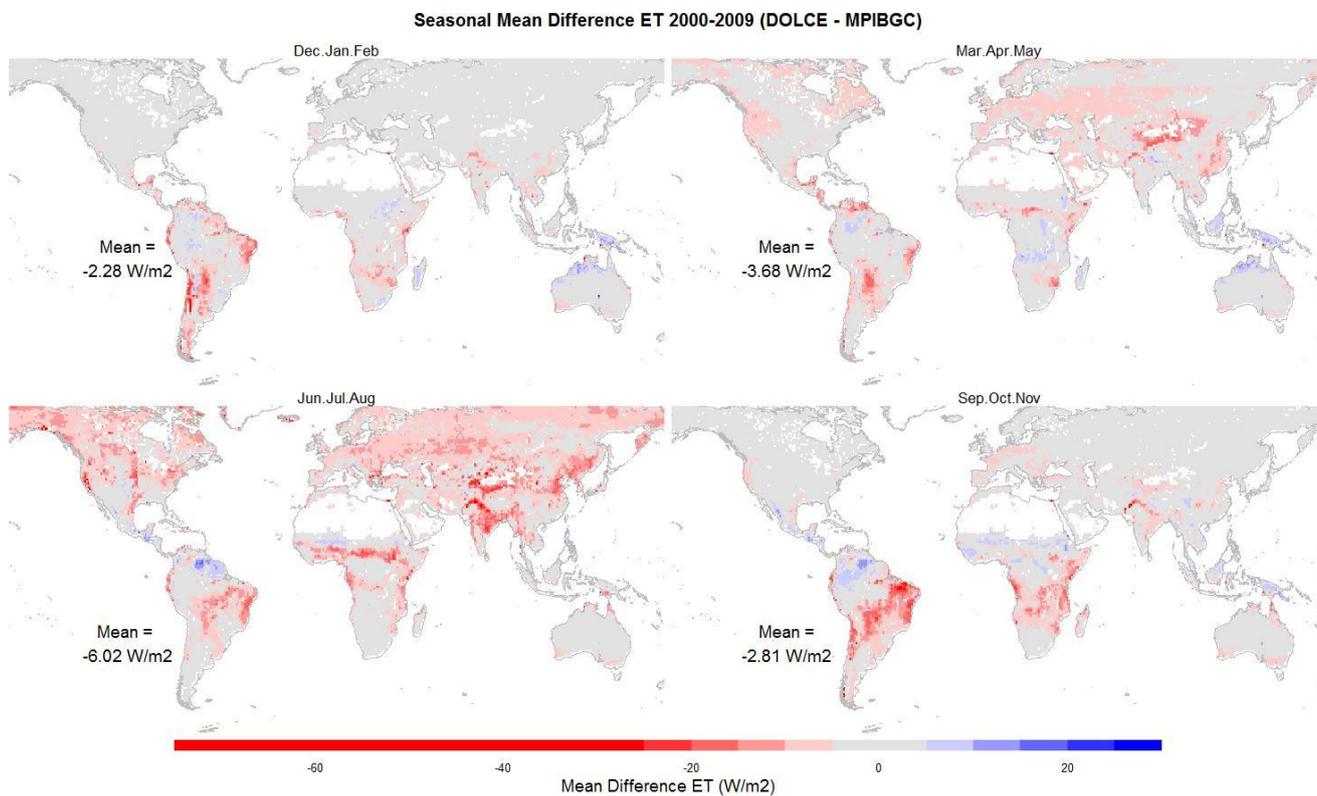
Figure 6: Difference between the seasonal average ET from MPIBGC and DOLCE calculated over the period 2000–2009.
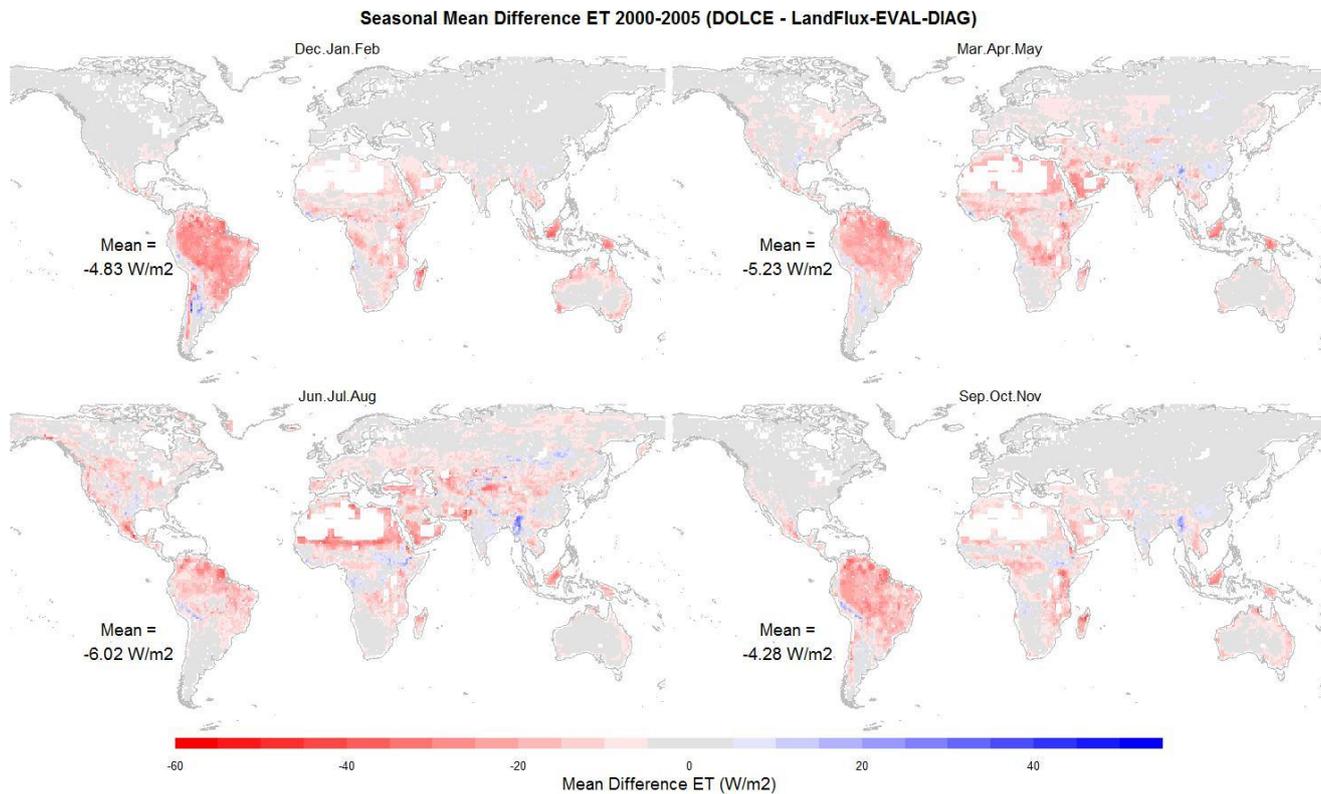
Figure 7: Difference between the seasonal average ET from LandFlux-EVAL-DIAG and DOLCE calculated over the period 2000–2005
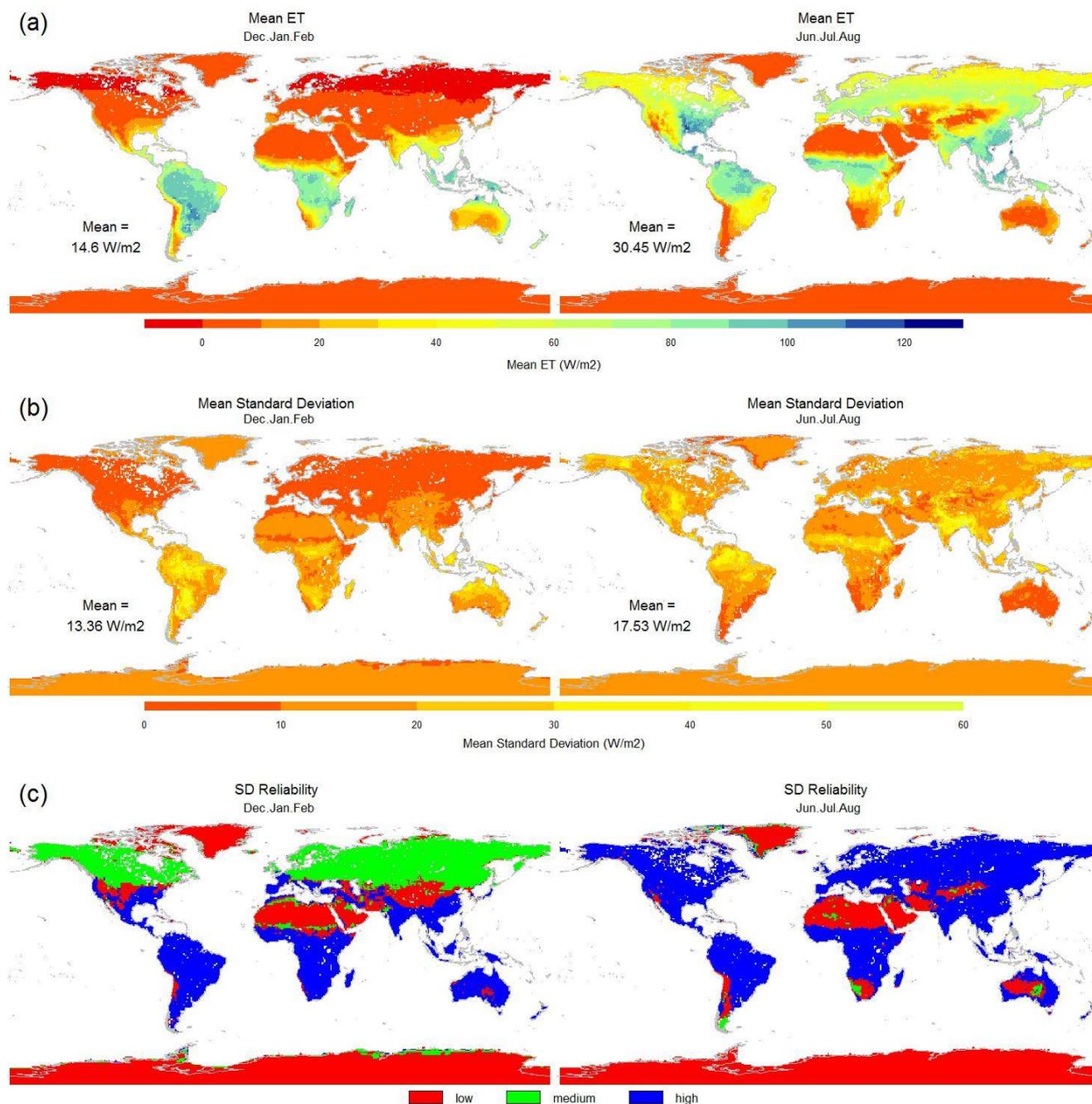
Figure 8: (a) Seasonal variability of global mean ET and (b) its associated uncertainty (standard deviation) showing their spatial distribution in Winter and Summer, (c) spatial distribution of the reliability of the uncertainty (standard deviation), showing regions where the reliability of uncertainty estimates is high ($\frac{\text{Uncertainty SD}}{\text{mean ET}} \leq 1$ in blue), medium($|\text{mean ET}| \leq 5$, Uncertainty SD < 10 and $\frac{\text{Uncertainty SD}}{\text{mean ET}} \geq 1$ in green) and low (in red).
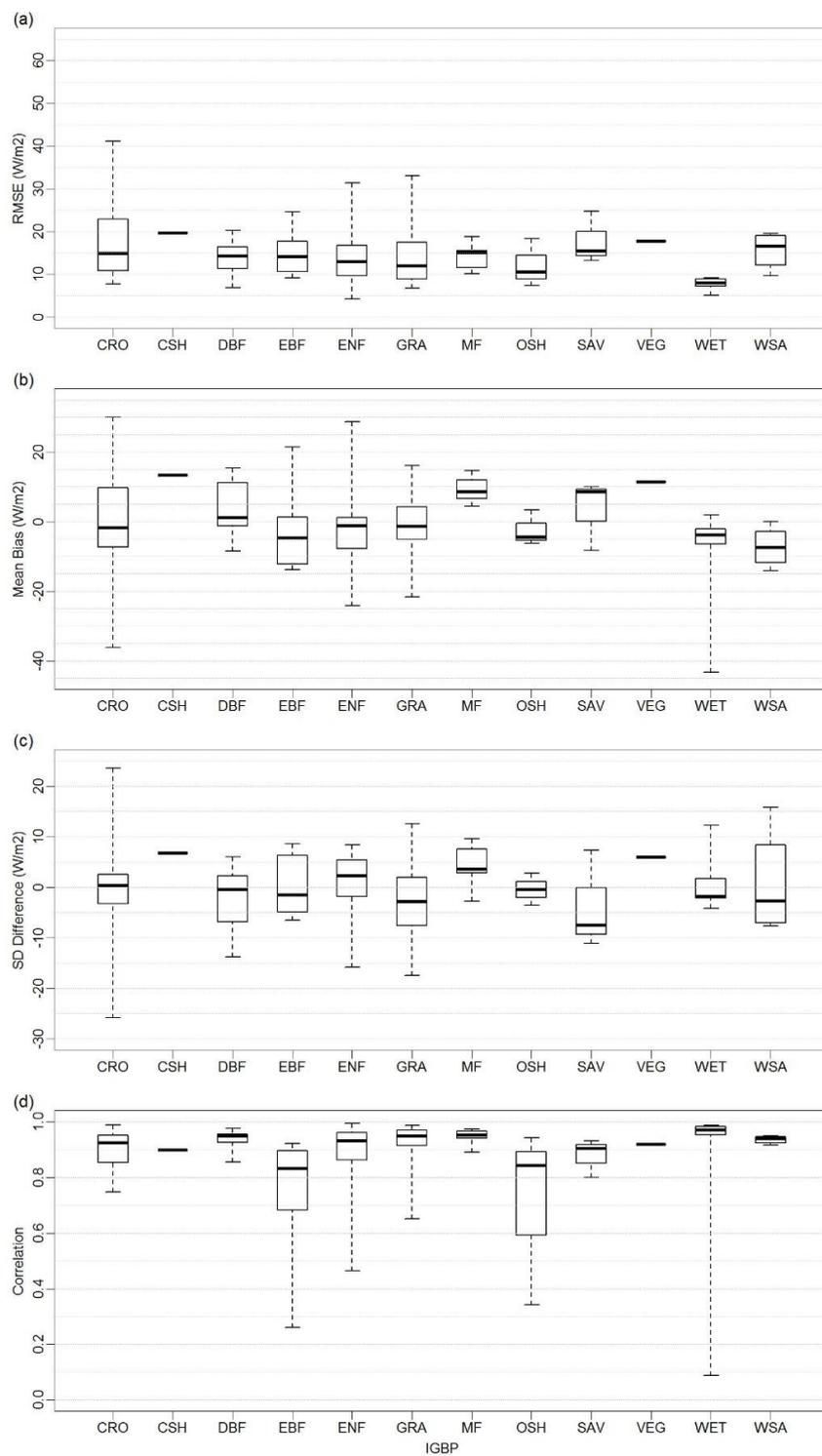
Figure 9: Four statistics, (a) RMSE, (b) Mean bias, (c) SD difference and (d) Correlation, calculated for DOLCE at 142 flux tower sites and displayed by biome types. See Fig. 2 for biome abbreviations.